ACS OMEGA

http://pubs.acs.org/journal/acsodf
Article

Nanopore Creation in Graphene at the Nanoscale for Water Desalination

Sidi Abdelmajid Ait Abdelkader,[†] Ismail Benabdallah,[†] Mohammed Amlieh,[†] and Abdelouahad El Fatimy*

Cite This: *ACS Omega* 2025, 10, 9113−9119
Read Online

ABSTRACT: Graphene-based 2D materials are renowned for their electrical, optical, magnetic, and mechanical properties. However, achieving stable, freestanding membranes for water desalination remains a major challenge. In response, we introduce a pioneering concept of a graphene device-based water filtration system. This system, featuring two graphene electrodes with nanopores, achieves the highest permeability value of 1208 L/h·m^2·bar while maintaining a 100% salt rejection due to the electric field. We present a straightforward method for controlling membrane pore sizes at the nanoscale using argon-plasma magnetron sputtering, demonstrating that the nanopores in graphene are controllable and potentially size-tunable. Furthermore, we enhance the membrane by incorporating two types of substrates, SiO_2 and SiC, making our concept more practical for industrial applications while preserving excellent desalination performances.

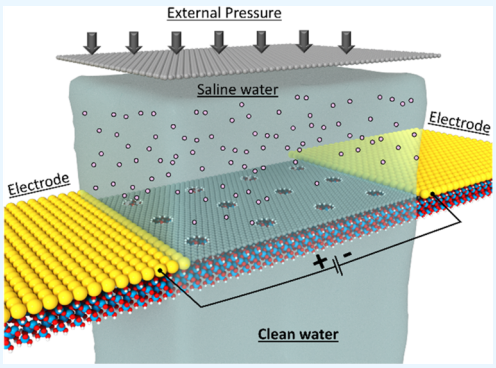

INTRODUCTION

Water scarcity is a critical global issue, with a staggering 4.0 billion people facing severe water scarcity for at least 1 month each year. This alarming statistic is a result of escalating water demand, diminishing water resources, and pollution driven by rapid population and economic growth. In this context, desalinating seawater is not just a solution but an urgent necessity, as it accounts for 97.5% of the planet's total water.[1,2] One of the most promising and energy-efficient technologies for desalination is reverse osmosis (RO). In this process, external hydrostatic pressure forces water through a porous membrane, making the permeable membrane a crucial element of the RO system.

Currently, polymeric membranes are widely used in reverse osmosis (RO) systems due to their desalination performance, characterized by a high water flux and effective salt rejection.[3] However, these membranes face significant challenges, such as slow water transport and irreversible membrane fouling.[4] To address these issues, extensive research has explored the potential of 2D materials as alternatives for RO membranes, including MoS_2, graphene, boron nitride (BN), and black phosphorus.[5] Among these materials, graphene-based membranes have garnered particular interest in the RO process.[6]

Graphene has an excellent potential to be used as an RO membrane due to its unique properties, such as mechanical and chemical stability, and its atomic thickness, which allows it to transport water faster than any conventional RO membrane, given that the water flux is scaling inversely to the membrane thickness.[7] Using molecular dynamics simulation, Cohen-Tanugi et al. reported that nanometer-scale pores in single-layer freestanding graphene could effectively filter NaCl salt from water.[8] The water permeability reported is about 2500 L/m^2·h·bar for the hydrogenated pore and 4167 L/m^2·h·bar for the hydroxylated pore with a salt rejection of about 70 and 45%, respectively, at a 150 MPa applied pressure.[8] Additionally, Cao et al., in their comparison of various types of 2D materials, reported a water permeance reaching 390 L/m^2·h·bar in the case of the MoS_2 membrane.[5] These values are several orders of magnitude higher than conventional reverse osmosis membranes.[8,9] Achieving a 100% salt rejection rate is crucial to enhancing the desalination performance, making it a significant challenge.

Here, we report a 100% salt rejection rate by adding an electric field while maintaining the same permeability values. Additionally, we demonstrate that incorporating a substrate with graphene allows the application of a higher pressure up to 1000 MPa. Furthermore, we introduce a straightforward nanofabrication technique and precise characterization to create pores in the nanoscale regime in the graphene membrane.

Received: September 27, 2024
Revised: December 26, 2024
Accepted: January 10, 2025
Published: February 27, 2025

https://doi.org/10.1021/acsomega.4c08852
ACS Omega 2025, 10, 9113−9119

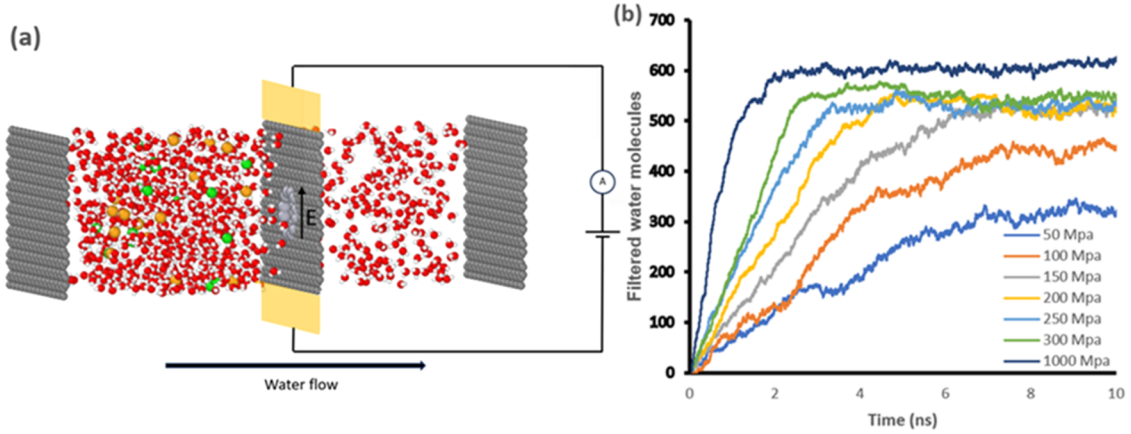

Figure 1. (a) Schematic of the proposed graphene device-based water filtration membrane. Green and orange atoms represent Na and Cl, respectively, while white and red atoms represent the water molecules. The 2E-NPG membrane is shown in the middle. (The yellow electrodes depict the presence of the applied electric field.) (b) Total number of filtered water molecules as a function of the simulation time for 2E-NPG at different applied pressures.

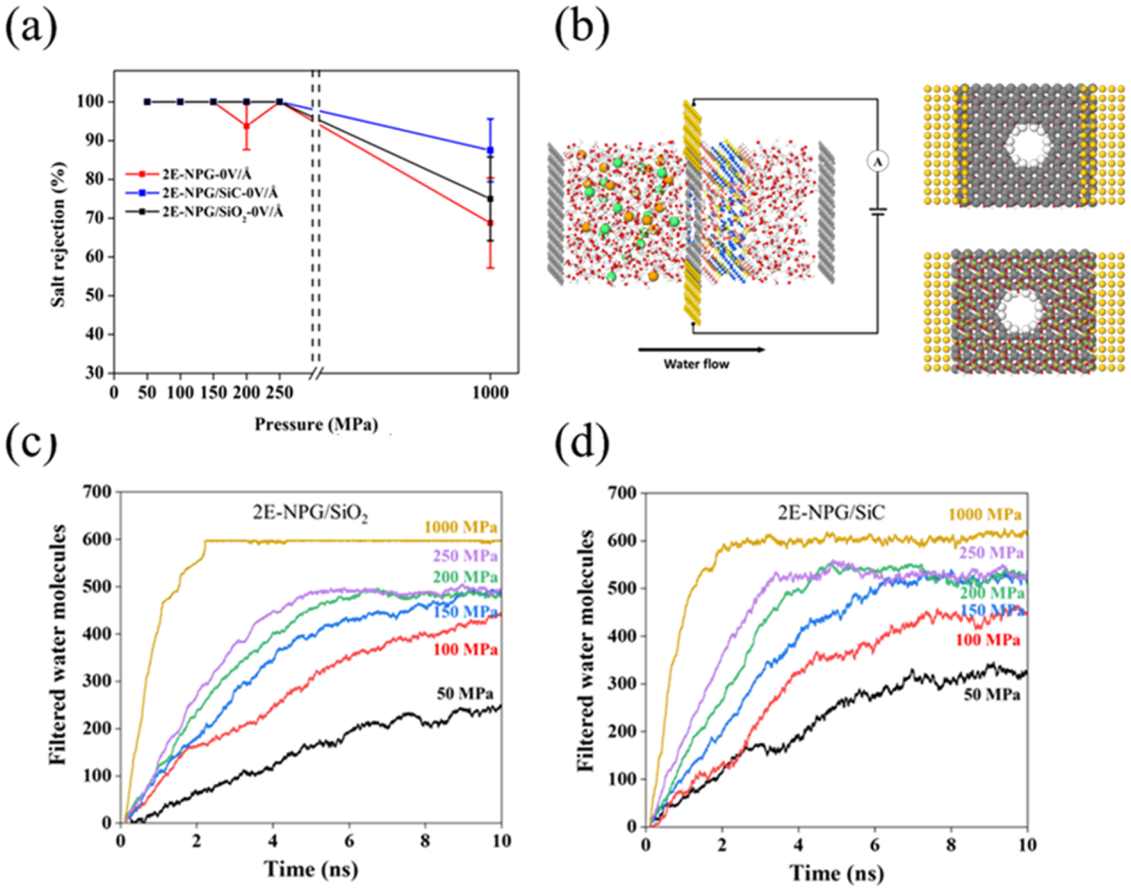

Figure 2. (a) Salt rejection as a function of pressure with no electric field. (b) Schematic of the proposed graphene/substrate device-based water filtration system. (c, d) Total number of filtered water molecules as a function of the simulation time for 2E-NPG/SiO_2 and 2E-NPG/SiC, respectively, at different applied pressures.

RESULTS AND DISCUSSION

Figure 1a shows the schematic concept of the filtration with the applied electric field parallel to the membrane named 2E-NPG. The 2E-NPG membrane is in the center of the simulation box. The right section contains an aqueous solution of water and NaCl with a salt concentration of 72 g/L, twice as high as seawater (~35 g/L); the pore size chosen is 0.81 nm to have comparable results with previous studies. The edges of the simulation box contain graphene pistons at which pressure is applied. It achieved permeability around 2015 L/m^2·h·bar for a pore size of 0.81 nm and 2708 L/m^2·h·bar for a 1 nm pore size with a 100% salt rejection.

Figure 1b shows the water flow rate through 2E-NPG as a function of time at different applied pressures from 50 MPa to 1 GPa without an applied electric field. The flow rate is constant over time and increases with the applied pressure;

https://doi.org/10.1021/acsomega.4c08852
ACS Omega 2025, 10, 9113−9119

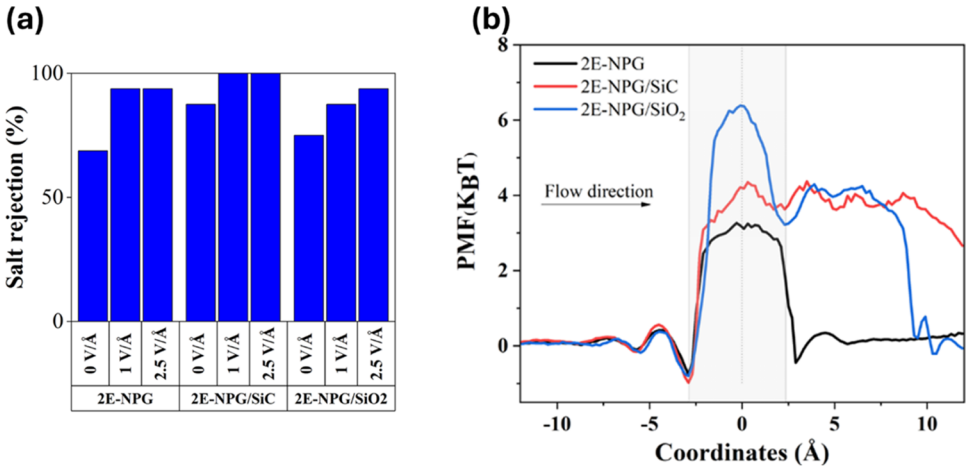

Figure 3. (a) Salt rejection as a function of applied electric fields for 1000 MPa. (b) Potential of mean force (PMF) of water molecules passing through the membranes from the saline to the permeate region.

each curve starts with a linear regime in which water molecules pass at a constant rate; then, each trajectory reaches a saturation level. The slope of each flow curve indicates the water flow rate over a certain period and is proportional to the applied pressure. The permeability parameter was calculated from the slope of the water flux as a function of pressure (Figure S1). The time intervals are 0−3 ns to remain in the transitory regime. The approximate permeability value for 2E-NPG is about 2015 L/h·m^2·bar.

To assess the passage of NaCl ions through the membrane, we calculated the salt rejection rate S_r from the following equation at different electric field values:[10]

$$S_r = \left(1 - \frac{N_p}{N_f}\right) \times 100$$

N_p and N_f are the percentage of salt in the permeate and feed regions at $t_{1/2}$, corresponding to the time when half of the water molecules have flowed to the permeate side at each given pressure (transitory regime). Salt rejection in desalination systems exhibits a dependence on the applied pressure. Simulation results, as presented in Figures 2a and 3a, show that at pressures ranging from 50 to 250 MPa, the system maintains a constant rejection rate of 100%. However, as the pressure increases, a noticeable decline in the salt rejection efficiency is observed. Specifically, at 1000 MPa, the salt rejection rate decreases to approximately 67%, which aligns with the findings reported by Cohen-Tanugi et al.[8] This reduction in efficiency at elevated pressures is attributed to the increased permeation of salt ions through the membrane, exceeding the membrane's selectivity barriers. However, the application of an electric field within the range of 1−2.5 V/Å has been shown to compensate for this effect; in fact, by integrating an electric field into the desalination process, the system can achieve 100% salt rejection at 1000 MPa, which significantly improves the membrane's efficiency. The figure contains the error bars, which are calculated using binomial distribution.

To propose a more realistic and mechanically robust membrane, we propose a novel water filtration membrane based on a two-electrode nanopore graphene membrane on a substrate. We studied the effect of substrates on the permeability and salt rejection values for the two-electrode graphene membrane with the nanopore based on SiO_2, named 2E-NPG/SiO_2, and SiC, named 2E-NPG/SiC. Using molecular dynamics simulation, we report a 100% salt rejection with maximum water permeabilities of about 1208 and 2333 L/m^2·h·bar for 2E-NPG/SiC for the hydrogenated pore size of about 0.8 nm and about 1 nm, respectively.

Figure 2b shows the schematic concept model of filtration with the applied electric field perpendicular to the water flow. The 2E-NPG/SiO_2 or 2E-NPG/SiC membrane is in the center of the simulation box. The calculation parameters are the same as those used for the 2E-NPG membrane.

Figure 2c,d shows the water flow rate through 2E-NPG/SiO_2 and 2E-NPG/SiC as a function of time at different applied pressures from 50 MPa to 1 GPa. Similarly, according to 2E-NPG results, the flow rate is constant over time and increases with the applied pressure, and the slope of each flow curve is proportional to the applied pressure. Considering the same duration and pressure, we note that 2E-NPG/SiC allows more water molecules to pass than does 2E-NPG/SiO_2. The approximate permeability value for 2E-NPG/SiO_2 is about 21.46 L/day·cm^2·MPa, which corresponds to 894.16 L/h·m^2·bar and 29.00 L/day·cm^2·MPa for 2E-NPG/SiC, which is equivalent to 1208 L/h·m^2·bar. For substrate-free 2E-NPG, the permeability obtained is 2015 L/h·m^2·bar. To assess the passage of NaCl ions inside the nanopore, we calculated the salt rejection using the same method that is explained in the first simulation.

As already discussed earlier (Figure 2a), the salt rejection rate without an applied electric field has a salt rejection of around 100% at low pressure, higher than in previous studies.[7] A free-substrate graphene membrane (2E-NPG) was also simulated as presented before, and for comparison, we found that the substrate enhances salt rejection. At a higher applied pressure (>250 MPa), the salt rejection decreases but is still significantly high for 2E-NPG/SiC as compared to 2E-NPG/SiO_2 or other reported NPG membranes.[6] Figure 3a shows the variation of salt rejection for applied electric fields for a pressure of 1000 MPa. As observed, the electric field enhances the salt rejection rate for the three membrane types, making it possible to have the highest permeability value while keeping a 100% salt rejection. In addition, incorporating a supportive substrate for the membrane like SiO_2 or SiC offers significant mechanical advantages, as highlighted in previous studies.[11] A substrate increases the overall thickness of the membrane,

https://doi.org/10.1021/acsomega.4c08852
ACS Omega 2025, 10, 9113−9119

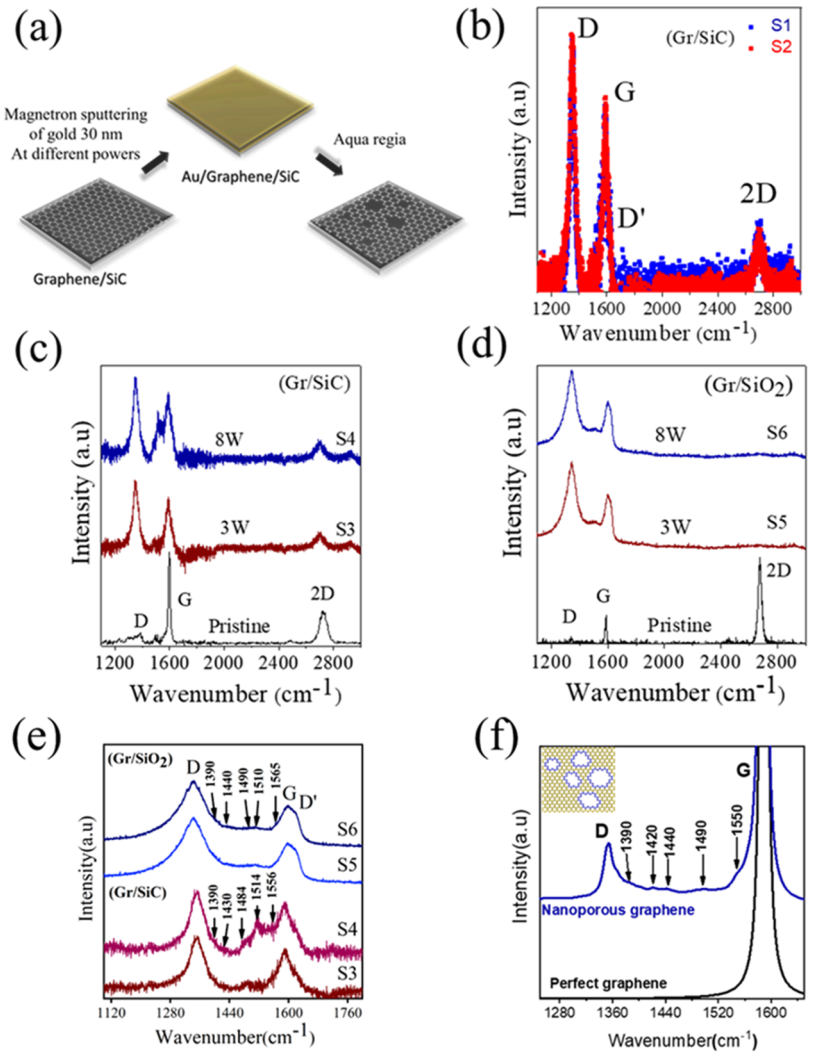

Figure 4. (a) Schematic illustration of the sample preparation process. (b) Measured Raman spectra of graphene on SiC of samples S_1 (blue) and S_2 (red). (c) Measured Raman spectra of graphene on SiC of samples S_3 (blue) and S_4 (red) and as-grown graphene on SiC (black). (d) Measured Raman spectra of graphene on SiO_2 of samples S_5 (blue) and S_6 (red) and as-grown graphene on SiO_2 (black). All Raman measurements are taken at E_L = 2.33 eV (λ_L = 532 nm). (e) Measured Raman spectra of samples S3, S4, S5, and S6 in the frequency range of 1100−1800 cm^{-1}. (f) Calculated Raman spectra of perfect graphene and graphene with nanopores. Inset: Schematic structure of graphene with nanopores. All Raman measurements are taken at E_L = 2.33 eV (λ_L = 532 nm).

thereby providing greater structural integrity and resistance to mechanical stresses.[11] This approach not only improves the functional performance of the desalination membrane but also enhances its feasibility for large-scale production and deployment in real-world applications.

To elucidate the efficiency of water molecule filtration near the membrane and substrate pores, we calculated the 2D average oxygen density (Figure S2). The distribution of water molecules near the pores dominates the water permeability and salt rejection. The pore size effects, substrate, electric field, and chemical effects of pore functionalization determine the water density. It was found that these densities in the vicinity of graphene are comparable for both substrates. However, these densities are different at the substrate level. To better understand the performance of each substrate on the permeability and salt rejection, we calculated the energy barrier that a water molecule needs to overcome to permeate. The energy barrier can be represented by the potential of mean force (PMF),[12] as shown in Figure 3b.

The PMF represents the mean force encountered by water molecules as they traverse the pore. In simpler terms, a higher PMF indicates that a water molecule needs greater energy to overcome the energy barrier and move into the permeate zone. The PMF was derived from the equilibrium density distribution using the following equation:[12]

$$\mathrm{PMF} = -k_B T \ln\left(\frac{\rho(z)}{\rho_0}\right)$$

where $\rho(z)$ is the bulk water density, ρ_0 is the local density, k_B is the Boltzmann constant, and T is the temperature. Figure 3b shows the PMF values. 2E-NPG exhibits the lowest PMF values, suggesting that water molecules are more likely to permeate through the membrane than a substrate. Interestingly, our findings reveal that the energy barrier scales proportionally with the permeability. Specifically, 2E-NPG/SiC, which exhibits higher permeability, has a lower PMF, while 2E-NPG/SiO_2, with lower permeability, shows a higher PMF. These PMF results align with the observed permeability,

https://doi.org/10.1021/acsomega.4c08852
ACS Omega 2025, 10, 9113−9119

concluding that the permeation mechanism is mainly governed by the energy barrier present across the membrane.

As such, we introduced a straightforward method to create nanopores at the nanoscale with a high efficiency. This is achieved by depositing a protective metal layer directly onto either as-grown graphene or graphene produced via chemical vapor deposition. We then conducted Raman spectroscopy on the resulting samples, which provided essential data on the nanopore sizes within the membranes. These measured nanopore diameters were subsequently employed in molecular dynamics (MD) simulations for the three types of membranes studied.

For that, we sputtered 30 nm of gold using argon-plasma magnetron sputtering with different powers, as shown in Figure 4a. Then, the deposited layer of the metal was subsequently removed by aqua regia.[13,14] This allows a one-step membrane fabrication process by protecting the two electrodes from aqua regia. Six graphene samples were processed: S_1, S_2, S_3, and S_4 correspond to ones grown on SiC, while S_5 and S_6 are deposited on the SiO_2 substrate.

Figure 4b shows the Raman spectra of samples S_1 and S_2, sputtered with the same power under the same conditions. The samples clearly show the presence of a large defect peak (D) at 1350 cm^{-1}, higher than the peak of G. The same I_D/I_G ratio (I_D/I_G = 1.3) in the Raman lines of S_1 and S_2 indicates that they contain the same defect concentration. This reveals the possibility of efficiently controlling the defect density in graphene.

The samples S_3 and S_5 (S_4, S_6) were treated by 3 W (8 W) sputtering powers, respectively. Figure 4c shows the Raman spectra for samples S_3 (red), S_4 (blue), and as-grown graphene (black). The spectra are represented after subtracting the SiC substrate Raman lines. As-grown graphene shows a small D-band and a low I_D/I_G ratio of about 0.1, which reveals high crystallinity. The sputtered samples show an intense D-band due to the defects generated during the sputtering process. The I_D/I_G ratio equals 1.5 and 1.4 for S_3 and S_4, respectively, and the spectrum shows small bands around 1450 and 1510 cm^{-1}.

Figure 4d depicts the Raman spectra for samples S_5 (red) and S_6 (blue) and as-grown graphene (black). Pristine graphene shows a small D-band, and the I_D/I_G ratio is approximately 0.12. Due to the disorder caused by the generated defects during the sputtering process, samples S_5 and S_6 show an intense D-band. The I_D/I_G ratio is, respectively, equal to 1.8 and 1.9. The Raman spectra of samples S_5 and S_6 clearly show the tiny band around 1450 cm^{-1}, as observed for samples S_3 and S_4. Such a band is already observed for defective graphene[15] and amorphous graphite thin films[16] and is often attributed to a third-order Raman mode of the silicon substrate.[17] However, this band is also observed for nanoporous graphene deposited on a poly-(ethylene terephthalate) foil.[18] Hence, this could be due to pores in graphene-based samples since it was observed for amorphous, defective, and nanoporous graphene.

We calculated the nonresonant Raman spectra of nanoporous monolayer graphene to estimate the size of vacancies created during sputtering. Several pore sizes were calculated and compared with the experimental Raman spectra. The pores were distributed randomly with a minimum distance of 30 Å to avoid interactions. The best fit to the experimental measured Raman spectra indicated nanopore sizes of about 7.5−12.5 Å, as assessed from Figure 4e.

Figure 4e,f represents the measured and calculated spectra for samples S3, S4, S5, and S6 for perfect and defective graphene in the 1100−1800 cm^{-1} frequency range. Good agreement was obtained between the measured and simulated data for the position of the D- and G-bands. The computed spectra show a small band around 1390, 1450, 1486, and 1510 cm^{-1}. The identification of these modes as local Raman modes due to the presence of pores in graphene was confirmed by calculating their associated eigen displacement vectors. Our computations show that as the distance between defects decreases, the bands merge into a single large band at around 1450 cm^{-1}, observed in the spectra of samples S5 and S6. This confirms that these bands are due to the pores in graphene rather than the SiO_2 substrate effects, as reported by different research groups.[15,16]

Further investigations into the morphologies of the 2E-NPG/SiC and 2E-NPG/SiO_2 membranes, including detailed SEM analysis, will be pursued to characterize the graphene defects fully. Additionally, mechanical simulations will be conducted to explore the substrate's role in providing support to the membrane.

In summary, we show that 2E-NPG/SiC and 2E-NPG/SiO_2 concepts with an applied electric field can reject 100% salt ions while letting water flow at permeabilities several orders of magnitude higher than those of existing RO membranes and are more realistic, efficient, and robust. We demonstrate that the nanopore size can be created and controlled by sputtering. Our results reveal that the pores in our samples have diameters ranging from 7.5 to 12.5 Å. Additionally, the Raman mode around 1450 cm^{-1}, previously attributed to the substrate effect in the literature, is due to defects in graphene. This work highlights the promise of graphene on a substrate for water desalination membranes. Our approach strongly suggests investigating low-dimensional materials for desalination membranes, which can yield significant improvements over existing membranes. This work will add substantial inputs to the next generation of membranes for clean water technology.

METHODS

Raman Simulation. The main parameters for the Raman spectra simulation are the dynamic matrix (D) and the polarizability tensor of the molecular system, which allow the determination of the Raman active mode's positions and their intensities. D describes the interactions between all atoms in the system; it has a $3N \times 3N$ dimension, where N is the number of atoms in the molecule. In practice, the system's symmetry can reduce the number of matrix variables to be calculated. In our case, the random distribution of the pores causes a low symmetrical aspect of the system. Hence, only the Hermitian character of D will be exploited. This requires computing all of the elements of D (diagonal and off-diagonal), which increases the computational time. Under these constraints associated with the critical number of atoms (in our case, 20,000 atoms), the diagonalization of the matrix becomes either impossible or requires a long computational time. However, the elements of our system's dynamic matrix are obtained using the constant force model introduced by Wirtz and Rubio,[19] which describes the interactions between the carbon atoms located away from the pores, while the interactions between the carbon atoms of the vacancy edges are calculated using density functional theory (DFT) as implemented in the SIESTA package.[20]

https://doi.org/10.1021/acsomega.4c08852
ACS Omega 2025, 10, 9113−9119

The Raman response is intimately related to molecular polarizability fluctuations. We used the bond polarizability model (BPM) to calculate the Raman line intensities.[21] This model is widely used to calculate the Raman spectra for different systems, and it shows perfect accuracy with the experimental results. The simulation of our Raman spectra is based on the spectral moment method (SMM). This allows us to calculate the Raman spectra without D diagonalization. The SMM, Raman equations, and computational details to derive the Raman susceptibility from the BPM are included in refs 22−24.

Molecular Dynamics Simulations. All simulations were performed with the LAMMPS package.[25] First, porous 2E-NPG/SiO_2 and 2E-NPG/SiC membranes were created. To do that, a careful scanning of the lattice parameter was done to ensure minimal mismatch between graphene and the substrate to respect the periodic boundary conditions. The system consisted of a finite box measuring 9 nm along the z direction and 2.8 and 3.25 nm along the x and y directions. The graphene membrane was fixed in the middle of the box at 4.5 nm. Six hundred water molecules were filtered with 16 Na and 16 Cl ions, corresponding to a salt concentration of 72 g/L. Two pistons represented by graphene sheets were placed on the box's top and bottom sides, with the piston's main role being to allow to push water toward the membrane at different external pressures. Pressures from 50 to 1000 MPa were applied to the piston.

Our simulations use the Moven Walls MW-NEMD approach, which captures the initial desalination process in nanoporous membranes under controlled flow conditions. The 10 ns simulation time is consistent with typical durations in similar molecular simulations of small nanopores, where a steady-state flow is often reached within shorter time scales. This is particularly relevant for systems where the transport behavior is dominated by the early stages of filtration, such as in the rapid desalination process through nanoporous materials.

Before running dynamics on our system, a minimization of the box size, followed by relaxation of water molecules, was allowed by using an NVT ensemble.

For the dynamics part, an NVT ensemble at a temperature of 300 K was used with a time step of 1 fs, which was deemed sufficient for reproducible results with good convergence. The total simulation time is up to 10 ns. To represent all of the interactions within our system, three potentials were used. The Tersoff potential was used for Si/O/H, the AIREBO potential was used for the carbon atoms and the functionalized hydrogen group, and Lennard-Jones TIP4P was used for water molecules and interatomic interactions. It should also be mentioned that the shape and size of the pore created in the membrane were chosen based on the experimental and Raman results, which suggest a circular form of our pores with a length of 1 nm. We used this simulation technique in our previous work on phosphorene numerical synthesis.[26]

■ ASSOCIATED CONTENT

Supporting Information

The Supporting Information is available free of charge at https://pubs.acs.org/doi/10.1021/acsomega.4c08852.

Molecular dynamics (MD) simulation methods, detailed calculations of water permeability and salt rejection rates, and the oxygen density map within the membrane pores. (PDF)

The proposed graphene device-based water filtration membrane. (MP4)

■ AUTHOR INFORMATION

Corresponding Author

Abdelouahad El Fatimy − *School of Applied and Engineering Physics, Mohammed VI Polytechnic University, Ben Guerir 43150, Morocco;* orcid.org/0000-0001-6500-7762; Email: Abdelouahed.ELFATIMY@um6p.ma

Authors

Sidi Abdelmajid Ait Abdelkader − *School of Applied and Engineering Physics, Mohammed VI Polytechnic University, Ben Guerir 43150, Morocco*

Ismail Benabdallah − *School of Applied and Engineering Physics, Mohammed VI Polytechnic University, Ben Guerir 43150, Morocco*

Mohammed Amlieh − *School of Applied and Engineering Physics, Mohammed VI Polytechnic University, Ben Guerir 43150, Morocco;* orcid.org/0009-0002-1454-0262

Complete contact information is available at: https://pubs.acs.org/10.1021/acsomega.4c08852

Author Contributions

†S.A.A.A., I.B., and M.A. contributed equally. A.E.F. designed the research concepts from the experimental approach to the simulation part. S.A.A.A. carried out the Raman simulation. I.B. and M.A. carried out molecular dynamics simulations. All authors discussed the results and wrote the paper.

Notes

The authors declare no competing financial interest.

■ ACKNOWLEDGMENTS

The OCP Foundation has supported this work with the project grant AS70, "Towards phosphorene-based materials and devices", and with the support of the Chair "Multiphysics and HPC" led by Mohammed VI Polytechnic University. We acknowledge the High-Performance Computing (HPC) Facility of Mohammed VI Polytechnic University, Toubkal.

■ REFERENCES

(1) Mekonnen, M. M.; Hoekstra, A. Y. Four billion people facing severe water scarcity. *Sci. Adv.* **2016**, *2* (2), No. e1500323.

(2) Boretti, A.; Rosa, L. Reassessing the projections of the world water development report. *NPJ Clean Water* **2019**, *2* (1), 15.

(3) Okamoto, Y.; Lienhard, J. H. How RO membrane permeability and other performance factors affect process cost and energy use: A review. *Desalination* **2019**, *470*, No. 114064.

(4) Mansouri, J.; Harrisson, S.; Chen, V. Strategies for controlling biofouling in membrane filtration systems: challenges and opportunities. *J. Mater. Chem.* **2010**, *20* (22), 4567−4586.

(5) Cao, Z.; Liu, V.; Farimani, A. Why is single-layer MoS2 a more energy efficient membrane for water desalination? *ACS Energy Lett.* **2020**, *5* (7), 2217−2222.

(6) Günay, M. G.; Kemerli, U.; Karaman, C.; Karaman, O.; Güngör, A.; Karimi-Maleh, H. Review of functionalized nano porous membranes for desalination and water purification: MD simulations perspective. *Environ. Res.* **2023**, *217*, No. 114785.

(7) Oviroh, P. O.; Jen, T. C.; Ren, J.; Mohlala, L. M.; Warmbier, R.; Karimzadeh, S. Nanoporous MoS2 membrane for water desalination: a molecular dynamics study. *Langmuir* **2021**, *37* (23), 7127−7137.

(8) Cohen-Tanugi, D.; Grossman, J. C. Water desalination across nanoporous graphene. *Nano Lett.* **2012**, *12* (7), 3602−3608.
(9) Homaeigohar, S.; Elbahri, M. Graphene membranes for water desalination. *NPG Asia Mater.* **2017**, *9* (8), e427.
(10) Sapkota, B.; Liang, W.; Vahid Mohammadi, A.; Karnik, R.; Noy, A.; Wanunu, M. High permeability sub-nanometre sieve composite MoS2 membranes. *Nat. Commun.* **2020**, *11* (1), No. 2747.
(11) Cohen-Tanugi, D.; Grossman, J. C. Mechanical strength of nanoporous graphene as a desalination membrane. *Nano Lett.* **2014**, *14* (11), 6171−6178.
(12) Yang, Y.; Li, W.; Zhou, H.; Zhang, X.; Zhao, M. Tunable C2N membrane for high efficient water desalination. *Sci. Rep.* **2016**, *6* (1), No. 29218.
(13) El Fatimy, A.; Han, P.; Quirk, N.; St Marie, L.; Marie, L. S.; Dejarld, M. T.; Myers-Ward, R. L.; Daniels, K.; Pavunny, S.; Gaskill, D. K.; Aytac, Y.; Murphy, T. E. Effect of defect-induced cooling on graphene hot-electron bolometers. *Carbon* **2019**, *154*, 497−502.
(14) Tsuda, Y.; Komori, T.; El Fatimy, A.; Horiike, K.; Suemitsu, T.; Otsuji, T. Application of plasmon-resonant microchip emitters to broadband terahertz spectroscopic measurement. *J. Opt. Soc. Am. B* **2009**, *26* (9), A52−A57.
(15) Cançado, L. G.; Jorio, A.; Ferreira, E. M.; Stavale, F.; Achete, C. A.; Capaz, R. B.; Moutinho, M. D. O.; Lombardo, A.; Kulmala, T. S.; Ferrari, A. C. Quantifying defects in graphene via Raman spectroscopy at different excitation energies. *Nano Lett.* **2011**, *11* (8), 3190−3196.
(16) Casiraghi, C.; Ferrari, A. C.; Ohr, R.; Chu, D.; Robertson, J. Surface properties of ultra-thin tetrahedral amorphous carbon films for magnetic storage technology. *Diam. Relat. Mater.* **2004**, *13* (4−8), 1416−1421.
(17) Kassab, L. R. P.; Santos, A. D. D.; Pillis, M. F. Evaluation of carbon thin films using Raman spectroscopy. *Mater. Res.* **2018**, *21*, No. e20170787.
(18) Fu, Y.; Su, S.; Zhang, N.; Wang, Y.; Guo, X.; Xue, J. Dehydration-determined ion selectivity of graphene subnanopores. *ACS Appl. Mater. Interfaces* **2020**, *12* (21), 24281−24288.
(19) Wirtz, L.; Rubio, A. The phonon dispersion of graphite revisited. *Solid State Commun.* **2004**, *131* (3−4), 141−152.
(20) Soler, J. M.; Artacho, E.; Gale, J. D.; García, A.; Junquera, J.; Ordejón, P.; Sánchez-Portal, D. The SIESTA method for ab initio order-N materials simulation. *J. Phys.: Condens. Matter* **2002**, *14* (11), 2745.
(21) Saito, R.; Takeya, T.; Kimura, T.; Dresselhaus, G.; Dresselhaus, M. S. Raman intensity of single-wall carbon nanotubes. *Phys. Rev. B* **1998**, *57* (7), 4145.
(22) Benoit, C.; Royer, E.; Poussigue, G. The spectral moments method. *J. Phys.: Condens. Matter* **1992**, *4* (12), 3125.
(23) Rahmani, A.; Sauvajol, J. L.; Rols, S.; Benoit, C. Nonresonant Raman spectrum in infinite and finite single-wall carbon nanotubes. *Phys. Rev. B* **2002**, *66* (12), No. 125404.
(24) Snoke, D. W.; Cardona, M.; Sanguinetti, S.; Benedek, G. Comparison of bond character in hydrocarbons and fullerenes. *Phys. Rev. B* **1996**, *53* (19), 12641.
(25) Thompson, A. P.; Aktulga, H. M.; Berger, R.; Bolintineanu, D. S.; Brown, W. M.; Crozier, P. S.; In't Veld, P. J.; Kohlmeyer, A.; Moore, S. G.; Nguyen, T. D.; Shan, R.; et al. LAMMPS-a flexible simulation tool for particle-based materials modeling at the atomic, meso, and continuum scales. *Comput. Phys. Commun.* **2022**, *271*, No. 108171.
(26) Tchoffo, D. B. T.; Benabdallah, I.; Aberda, A.; Neugebauer, P.; Belhboub, A.; El Fatimy, A. Large-scale synthesis of defect-free phosphorene on nickel substrates: enabling atomistic thickness devices. *J. Phys. D: Appl. Phys.* **2024**, *57* (43), No. 435302.

https://doi.org/10.1021/acsomega.4c08852
ACS Omega 2025, 10, 9113−9119